Anelasticity Study on Motions of Atoms in the Grain Boundary Regions in Nanocrystalline Gold

doi: 10.2320/matertrans.44.53

Materials Transactions, Vol. 44, No. 1 (2003) pp. 53 to 58
Special Issue on Diffusion in Materials and Its Application —Recent Development—

Anelasticity Study on Motions of Atoms in the Grain Boundary Regions in Nanocrystalline Gold

Hisanori Tanimoto[1,2,*1], Seiji Sakai[1,*2] and Hiroshi Mizubayashi[1]

[1]*Institute of Materials Science, University of Tsukuba, Tsukuba 305-8573, Japan*
[2]*Center of Tsukuba Advanced Research Alliance (TARA), University of Tsukuba, Tsukuba 305-8573, Japan*

High-density nanocrystalline (n-) Au was prepared by the gas deposition method. Various anelastic and plastic creep processes associated with the grain boundary (GB) regions were observed. The vibrating reed measurements at 10^2 Hz with strain amplitude of 10^{-6} show a very broad internal friction peak near 95 K, $Q^{-1}_{p,95\,K}$, and a steep increase in the anelastic strain above 200 K, $\varepsilon_{a\text{-}I,>200\,K}$. The tensile tests show a steep increase in the anelastic strain above 200 K, $\varepsilon_{a\text{-}II,>200\,K}$, for the stress beyond a few MPa and a linear plastic creep strain above 200 K, $\varepsilon_{pc\text{-}1}$, for stress range between 30 MPa and 150 MPa. The activation parameters, $1/\tau_0$ of 3×10^{11} s^{-1} and E of 0.16 eV, are found for $Q^{-1}_{p,95\,K}$, where τ_0 and E are a pre-exponential factor and an activation energy of the relaxation time τ. We surmise that simple relaxation processes are responsible for $Q^{-1}_{p,95\,K}$. The values of $1/\tau_0$ and E found for $\varepsilon_{a\text{-}I,>200\,K}$ and $\varepsilon_{a\text{-}II,>200\,K}$ decrease with increasing the applied stress or the temperature, indicating that their atomic processes are the same feather. Further, E found for $\varepsilon_{pc\text{-}1}$ is similar to or slightly smaller than that of $\varepsilon_{a\text{-}II,>200\,K}$. These observations indicate that the atomic motions in the GB regions of n-Au develop in scale in the order of the underlying processes for $\varepsilon_{a\text{-}I,>200\,K}$, $\varepsilon_{a\text{-}II,>200\,K}$ and $\varepsilon_{pc\text{-}1}$, and are so different from those in the conventional polycrystalline Au.

(Received September 3, 2002; Accepted November 11, 2002)

Keywords: *nanocrystalline metal, gas-deposition method, grain boundary, diffusion, cooperative motion*

1. Introduction

Nanocrystalline (n-) materials can be considered as composite materials consisting of grain boundary regions and crystallites of nanometer scale.[1)] The considerably low elastic modulus[2,3)] and the high-diffusivity being close to the surface diffusion[4,5)] were reported in the pioneer works of n-metals. However, these may be associated with pores contained in the specimens at the dawn of the studies. With progress in the preparation method of n-metal specimens, it is found that the elastic modulus of pore-free or high-density n-metals[6–9)] is very close to that of the conventional polycrystalline (p-) metals. The activation energy found for tracer diffusivity in the high-density n-metals is almost the same as that reported for the GB diffusion in the p-metals.[10–12)] A steep increase in the internal friction, Q^{-1}, of n-metals is observed at the temperature slightly higher than 300 K, where the activation energy estimated is also close to that reported for the GB diffusion in p-metals.[13–20)] These results indicate that intrinsic natures of the GB regions in n-metals appear to be similar to those in p-metals.

On the other hand, an anelastic response of n-gold (n-Au) found near or below room temperature is different from that of p-Au. Figure 1(a) shows an example of the Q^{-1} observed in n-Au, where a broad peak at around 95 K ($Q^{-1}_{p,95\,K}$, hereafter) and a steep increase above about 200 K ($Q^{-1}_{>200\,K}$, hereafter) can be seen.[8)] Both $Q^{-1}_{p,95\,K}$ and $Q^{-1}_{>200\,K}$ diminish after the grain growth[9)] and remain unchanged after the low temperature irradiation.[21,22)] As well as that neither $Q^{-1}_{p,95\,K}$ nor $Q^{-1}_{>200\,K}$ are observed in p-Au, these observations indicate that they are associated with anelastic processes in the GB regions. In the following, we will refer to the elastic strain, anelastic strain and plastic strain as ε_e, ε_a and ε_p, respectively.

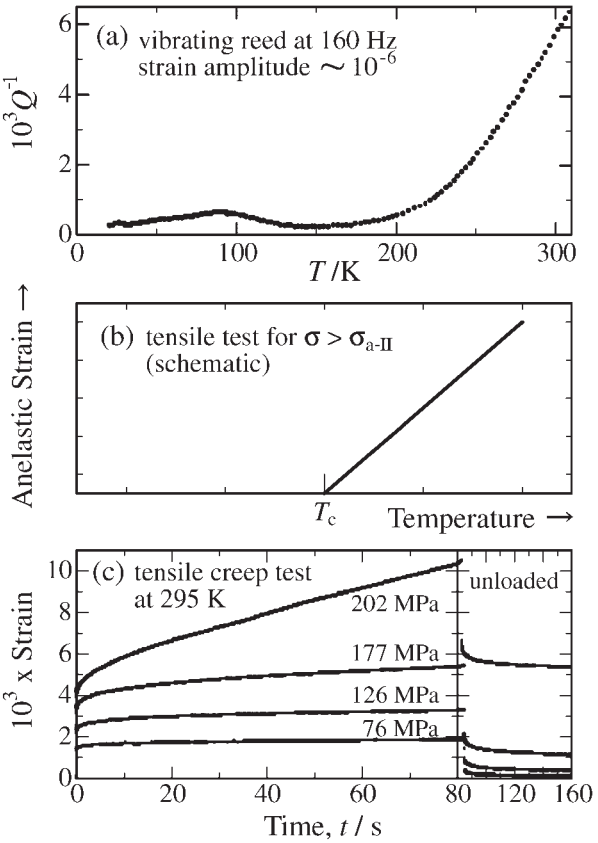

Fig. 1 (a) Example of the internal friction observed in the type-H n-Au specimen with the mean grains size of about 30 nm.[8)] (b) Schematic drawing for the anelastic strain $\varepsilon_{a\text{-}II,>200\,K}$ found in n-Au for the applied stress σ higher than the threshold stress $\sigma_{a\text{-}II}$ of a few MPa.[23,24)] (c) Examples for the tensile creep tests of the type-H n-Au specimens at 295 K.[25)]

In Fig. 1(a), one can assume that constitutional anelastic strains $\varepsilon_{a,95\,K}$ and $\varepsilon_{a\text{-}I,>200\,K}$ are responsible for $Q^{-1}_{p,95\,K}$ and $Q^{-1}_{>200\,K}$, respectively, where the ratios $\varepsilon_{a,95\,K}/\varepsilon_e$ and

*1Corresponding author: E-mail: tanimoto@ims.tsukuba.ac.jp
*2Present address: Takasaki-branch, Advanced Science Research Center, Japan Atomic Energy Research Institute, Takasaki 370-1292, Japan.

$\varepsilon_{\text{a-I},>200\,\text{K}}/\varepsilon_{\text{e}}$ are the order of 10^{-3} at the applied stress of 0.1 MPa. Figure 1(b) is a schematic drawing for the anelastic strain $\varepsilon_{\text{a-II},>200\,\text{K}}$ found in n-Au for the applied stress σ higher than the threshold stress $\sigma_{\text{a-II}}$ of a few MPa, where $\varepsilon_{\text{a-II},>200\,\text{K}}$ manifests at temperatures higher than the threshold temperature $T_{\text{a-II}}$ of about 200 K.[23,24] The empirical relationship given by

$$\varepsilon_{\text{a-II},>200\,\text{K}} = C_{\text{a-II}} J_{\text{a-II}} (\sigma - \sigma_{\text{a-II}})(T - T_{\text{a-II}}) \tag{1}$$

is found, where $J_{\text{a-II}}$ is the anelastic compliance responsible for $\varepsilon_{\text{a-II},>200\,\text{K}}$ and $C_{\text{a-II}}$ is the temperature coefficient of $\varepsilon_{\text{a-II},>200\,\text{K}}$.[25] It is noted that the ratio $\varepsilon_{\text{a-II},>200\,\text{K}}/\varepsilon_{\text{e}}$ increases beyond unity at applied stresses above 10 MPa and temperatures above room temperature.[25] In the stress range beyond a few tens MPa and in the temperature range near or above the room temperature, the plastic creep deformation of n-Au can be observed. Figure 1(c) shows examples for the tensile creep tests of the type-H (see below for the type-H and type-L) n-Au specimens at 295 K, where the steady state creep rate $(\text{d}\varepsilon/\text{d}t)_{\text{pc-1}}$ is found to be explained by

$$(\text{d}\varepsilon/\text{d}t)_{\text{pc-1}} = (\text{d}\varepsilon/\text{d}t)_{\text{pc-1,0}} (\sigma - \sigma_{\text{pc-1}}) \exp(-E_{\text{pc-1}}/kT) \quad \text{for} \quad \sigma_{\text{pc-1}} \le \sigma < \sigma_{\text{pc-2}} \tag{2}$$

where $E_{\text{pc-1}}$ is the activation energy for the plastic creep observed in the stress region-1 between $\sigma_{\text{pc-1}}$ and $\sigma_{\text{pc-2}}$, and k denotes the Boltzmann constant. At the room temperature, $\sigma_{\text{pc-1}}$ and $\sigma_{\text{pc-2}}$ are about 30 and 150 MPa for the type-H n-Au specimens, and about 60 and 300 MPa for the type-L n-Au specimens, respectively.[25] That is, the atoms contained in the GB regions of n-Au undergo various motions as a function of the applied stress, which may give interesting insight into characteristics of the atomic migration in n-metals. In the present work, we investigated $\varepsilon_{\text{a,95\,K}}$, $\varepsilon_{\text{a-I},>200\,\text{K}}$, $\varepsilon_{\text{a-II},>200\,\text{K}}$ and $(\text{d}\varepsilon/\text{d}t)_{\text{pc-1}}$ from this point of view.

2. Experimental Procedure

High-density n-Au specimens were prepared by applying the gas-deposition (GD) method.[8] The GD apparatus is composed of an evaporation chamber, a deposition chamber, a transfer pipe connecting the two chambers and a helium circulation system with purification columns. Ultra-fine Au particles formed by the inert-gas condensation process in the evaporation chamber were sucked by the transfer pipe and transferred onto a cooled glass substrate in the deposition chamber. The purity of the helium gas was kept as high as 99.9999% in order to obtain contamination-free and fully-dense specimens. Ribbon like specimens of 23 mm long and 1 mm wide were prepared by controlling the position of the substrate. After the deposition, the specimens were carefully removed from the glass substrate, where no bending and breaking of the specimens were found. Typical thickness of the specimens was about 20 μm. The density measured by the Archimedes' method was $19.4 \pm 0.2\,\text{g/cm}^3$ for all the specimens, which shows good agreement with $19.32\,\text{g/cm}^3$ reported for the bulk Au value in literature. The mean grain size, d, measured from the STM surface topography and the peak broadening of X-ray diffraction (XRD) peaks was about 20–30 nm.

The n-Au specimens prepared by the GD method are classified into two groups, the type-L and type-H specimens prepared with the low and high deposition rates of the ultra-fine particles, respectively.[8,9] We surmise that some spontaneous reorientation of the ultra-fine particles takes place on the specimen surface just after the landing of the ultra-fine particles, resulting in that the reorientation is completed in the type-L specimens but not in the type-H specimens. The density of the n-Au specimens is the same between the type-L and type-H specimens, but the crystallographic distribution of the constituent n-crystallites is somewhat different between the type-L and type-H specimens. In the present work, most of the specimens used are the type-H n-Au specimens. We carried out the vibrating reed measurements in the frequency range of 10^2 Hz with the strain amplitude of 10^{-6}, and the tensile tests in the stress range above a few MPa.

3. Results

Figures 2(a) and (b) are the enlarged drawings of Fig. 1(a). As seen in Fig. 2(a), $Q^{-1}_{\text{p,95\,K}}$ is observed as a broad peak accompanied by low temperature shoulders, where the peak temperature T_{p} of the dominant peak is investigated as a function of the measurement frequency f. In Fig. 2(b), except for the transient increase near 200 K, the most part of $Q^{-1}_{>200\,\text{K}}$ can be given by

$$Q^{-1}_{>200\,\text{K}} = C_{\text{a-I,Q}} (T - T_{\text{a-I}}) \tag{3}$$

where $T_{\text{a-I}}$ is the threshold temperature and $C_{\text{a-I,Q}}$ is the temperature coefficient. Then, $\varepsilon_{\text{a-I},>200\,\text{K}}$ may be given by

$$\varepsilon_{\text{a-I},>200\,\text{K}} = C_{\text{a-I}} J_{\text{a-I}} \sigma (T - T_{\text{a-I}}) \tag{4}$$

where $J_{\text{a-I}}$ is the anelastic compliance responsible for $\varepsilon_{\text{a-I},>200\,\text{K}}$ and $C_{\text{a-I},\varepsilon}$ is the temperature coefficient. The threshold temperature $T_{\text{a-I}}$ is about 200 K, where $T_{\text{a-I}}$ is

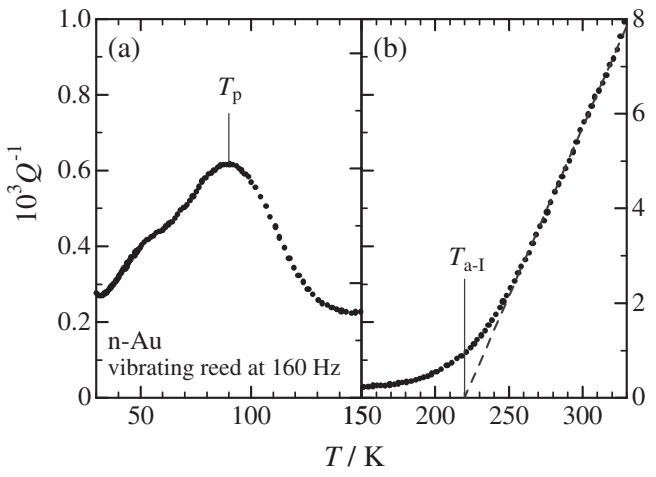

Fig. 2 (a) and (b) are the enlarged drawings of Fig. 1(a).

investigated as a function of f.

Figure 3 shows the f dependence of T_p (the peak temperature of $Q^{-1}_{p,95\,K}$) observed for the type-H n-Au specimens. In the analysis, we assumed that the relationship of $2\pi f \cdot \tau = 1$ is found at T_p, where the apparent relaxation time τ for $Q^{-1}_{p,95\,K}$ can be denoted as

$$\tau = \tau_0 \exp(E/kT). \quad (5)$$

In eq. (5), τ_0 and E are the pre-exponential factor and the activation energy. In Fig. 3, $1/\tau_0$ of $\sim 3 \times 10^{11}\,s^{-1}$ and E of $\sim 0.16\,eV$ ($1\,eV = 1.602 \times 10^{-19}\,J$) are found for $Q^{-1}_{p,95\,K}$. It is noted that these values are slightly lower than $1/\tau_0$ of 10^{12}–$10^{13}\,s^{-1}$ and E of 0.2 eV reported for the Bordoni peak of the deformed p-Au specimens.[26)]

Figure 4 shows the f dependence of $T_{a\text{-}I}$ (the threshold temperature for $Q^{-1}_{>200\,K}$), where $1/\tau_0$ ($=2\pi f_0$) of $\sim 9 \times 10^{14}\,s^{-1}$ and E of $\sim 0.57\,eV$ are found. These values are compiled in Table 1.

Figure 5 shows examples of the tensile tests for the type-H

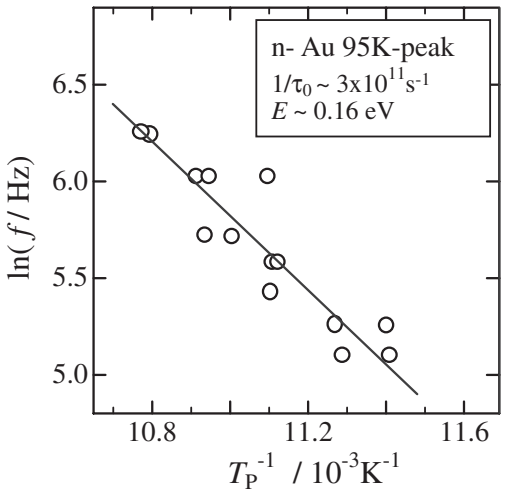

Fig. 3 Frequency f dependence of the peak temperature T_p of the $Q^{-1}_{p,95\,K}$ observed for the type-H n-Au specimens.

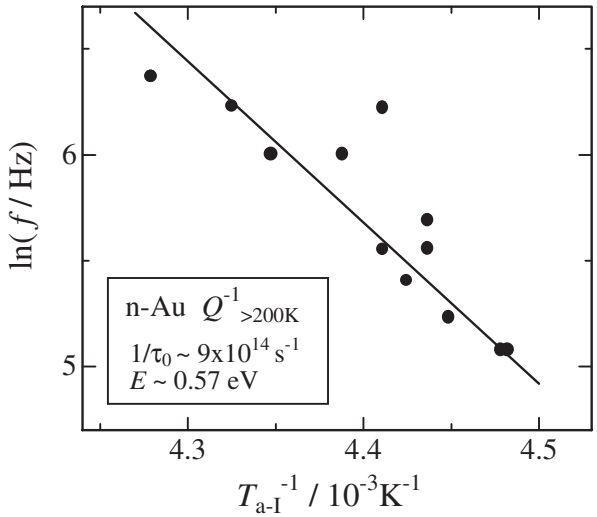

Fig. 4 Frequency f dependence of the threshold temperature $T_{a\text{-}I}$ for $Q^{-1}_{>200\,K}$.

Table 1 Activation parameters for various anelastic processes and the linear plastic creep process found for n-Au.

Process	$1/\tau_0$ (s^{-1})	E (eV)	Remarks
$Q^{-1}_{p,95\,K}$ or $\varepsilon_{a,95\,K}$	3×10^{11}	0.16	
$Q^{-1}_{>200\,K}$ or $\varepsilon_{a\text{-}I,>200\,K}$	9×10^{14}	0.57	
$\varepsilon_{a\text{-}II,>200\,K}$			$\sigma >$ a few MPa
near 250 K	2×10^{9}	0.53	
near 270 K	2×10^{7}	0.46	
near 300 K	5×10^{4}	0.39	
linear plastic creep			
at 145 MPa		0.36	at room temperature type-H n-Au: 30 MPa $< \sigma <$ 150 MPa type-L n-Au: 60 MPa $< \sigma <$ 300 MPa
at 200 MPa		0.55	

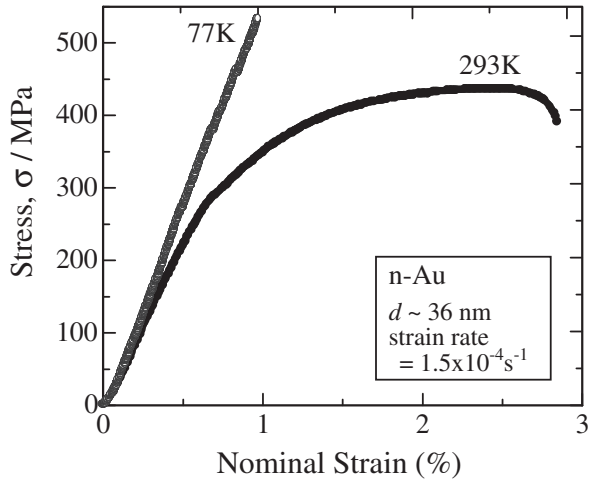

Fig. 5 Examples of the tensile tests for the type-H specimens.[8)]

n-Au specimens,[8)] where the tensile test at 77 K was interrupted at the strain of 1% to avoid the yielding. To pursue the relaxation parameters for $\varepsilon_{a\text{-}II,>200\,K}$, the stress relaxation tests were conducted. The tensile tests were interrupted at a given applied stress σ_0, and then the decrease in the stress under the constant strain was measured as a function of the elapsed time. Figure 6 shows examples of stress relaxation curves observed for the type-H n-Au specimens, where no stress relaxation is detected at 103 K and a considerable stress relaxation above 200 K. The whole stress relaxation curve is not explained by a single relaxation process, indicating that the relaxation time for the stress relaxation has a distribution or different atomic processes are overlapped. In order to get insight into the atomic processes, we assumed that the observed stress relaxation curve can be explained by the superposition of discrete single relaxation curves. Figure 7 is the redrawing of the stress relaxation curve at 298 K shown in Fig. 6, where shown is an example of the decomposition with the constituent relaxations 2 to 4. In Fig. 7, the constituent relaxation 4 is determined as that with the longest relaxation time, and then the constituent relaxation 3 is determined after the subtraction of the constituent relaxation 4, and so on for the constituent relaxation 2. Similar procedures were made for other stress

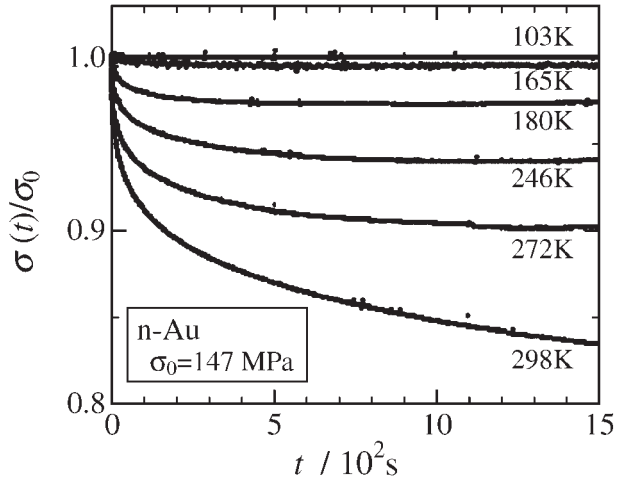

Fig. 6 Stress relaxation tests after the tensile tests up to the applied stress σ_0 of 147 MPa, which were observed for the type-H n-Au specimens.

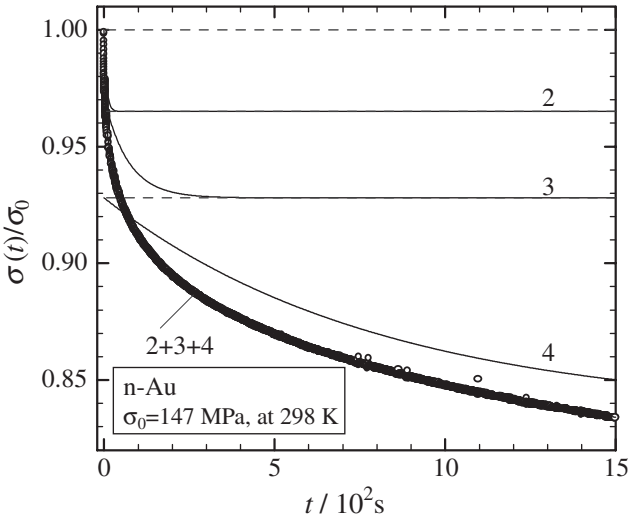

Fig. 7 Redrawing of the stress relaxation curve at 298 K shown in Fig. 6, but here an example of the decomposition to the constituent relaxations 2 to 4 is shown.

relaxation curves shown in Fig. 6. For example, the stress relaxation curve at 272 K can be explained by the constituent relaxations 1 to 3, where the constituent relaxation 4 is not detected because the relaxation time is too long to be detected in the time scale shown in Fig. 6. It is noted that the present decomposition into the constituent relaxations corresponds with a snapshot in the temperature and time scale, here the snapshot at 298 K is taken as the reference. In the present analysis, the fractional strengths of the constituent relaxations activated in the time scale of 15 ks were almost constant between the results observed from 246 to 298 K. Figure 8 shows the relaxation times of the constituent relaxations as a function of the temperature, where the relaxation parameters for the stress relaxation 1 activated near 250 K are $1/\tau_0 \sim 2 \times 10^9\,\mathrm{s}^{-1}$ and $E \sim 0.53\,\mathrm{eV}$, those for 2 near 270 K are $1/\tau_0 \sim 2 \times 10^7\,\mathrm{s}^{-1}$ and $E \sim 0.46\,\mathrm{eV}$, and those for 3 near 300 K are $1/\tau_0 \sim 5 \times 10^4\,\mathrm{s}^{-1}$ and $E \sim 0.39\,\mathrm{eV}$. Various factors are contained in the apparent $1/\tau_0$ obtained from Figs. 3, 4 and 8. However, the $1/\tau_0$ for the stress

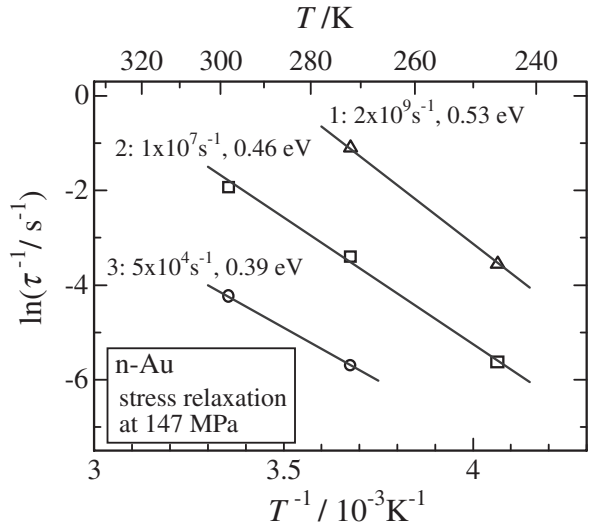

Fig. 8 Relaxation times of the constituent stress relaxations as a function of the temperature.

relaxation 3 is much lower than those of $\varepsilon_{a,95\,K}$ and $\varepsilon_{a\text{-}I,>200\,K}$, indicating that the corresponding attempt frequency is much lower than that of $\varepsilon_{a,95\,K}$ and $\varepsilon_{a\text{-}I,>200\,K}$.

As already shown in Fig. 1(c), the plastic creep strain can be detected for the long term tests under the applied stress beyond $\sigma_{pc\text{-}1}$ which is about 30 MPa for the type-H n-Au specimens. Figure 9 shows examples for the steady state creep rate $(d\varepsilon/dt)_{pc\text{-}1}$ observed for the type-H specimens as a function of temperature. The data fitted with the solid lines correspond with the linear creep range explained by the empirical relationship (2), and the data fitted with the dashed lines correspond with the variable effective-grain-size creep[25] which is out of the present scope. The activation energy $E_{pc\text{-}1}$ found is 0.36 eV and 0.55 eV for the applied stress of 145 MPa and 200 MPa, respectively.

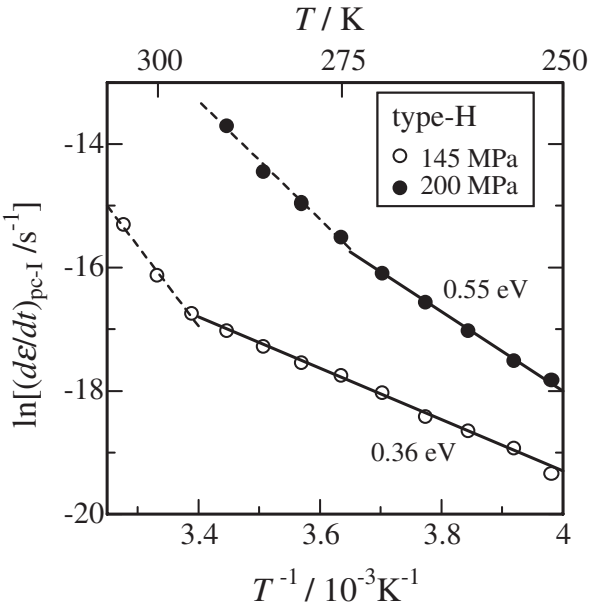

Fig. 9 Examples for the steady state creep rate ($d\varepsilon/dt$) observed for the type-H specimens as a function of temperature.

4. Discussion

Table 1 shows the activation parameters found for the various anelastic processes and the linear plastic creep process which are associated with the atomic motions in the GB regions of n-Au. For the anelastic processes at the lowest temperatures responsible for $Q^{-1}_{p,95\,K}$ or $\varepsilon_{a,95\,K}$, the activation parameters $1/\tau_0$ of $3 \times 10^{11}\,s^{-1}$ and E of 0.16 eV may be explained by a simple relaxation process, and a broadness of the 95 K peak may reflect variety of the GB structures. The activation energy found for $Q^{-1}_{p,95\,K}$ or $\varepsilon_{a,95\,K}$ is much lower than that of 0.88 eV reported for the GB diffusion in p-Au,[27] suggesting that some structural relaxations in the GB regions in n-Au are responsible for $Q^{-1}_{p,95\,K}$ or $\varepsilon_{a,95\,K}$.

The anelastic processes responsible for $Q^{-1}_{>200\,K}$ or $\varepsilon_{a\text{-}I,>200\,K}$ and $\varepsilon_{a\text{-}II,>200\,K}$, and the plastic creep process which are revealed with increasing the applied stress may be the same feather. As mentioned for Fig. 7, the characteristic temperature dependence of $\varepsilon_{a\text{-}II,>200\,K}$ shown in the empirical relationship (1) is associated with the distribution of the relaxation times of the constituent anelastic processes. Although the precious distribution is not known, the result shown in Fig. 8 suggests that both the activation parameters $1/\tau_0$ and E of the individual anelastic process decrease for the anelastic processes which can be activated at the higher temperatures. It should be the case for $Q^{-1}_{>200\,K}$ or $\varepsilon_{a\text{-}I,>200\,K}$ too, because the temperature dependence of $Q^{-1}_{>200\,K}$ or $\varepsilon_{a\text{-}I,>200\,K}$ shown in the empirical relationship (3) or (4) is very similar to the eq. (1) for $\varepsilon_{a\text{-}II,>200\,K}$. Then the activation parameters $1/\tau_0$ of $9 \times 10^{15}\,s^{-1}$ and E of 0.57 eV found for the threshold temperature of $Q^{-1}_{>200\,K}$ or $\varepsilon_{a\text{-}I,>200\,K}$ are their ultimate values for the constituent anelastic process activated at the lowest temperature.

Since simple relaxation processes may be completed after the $Q^{-1}_{p,95\,K}$ or $\varepsilon_{a,95\,K}$, some process associated with plural atoms should be responsible for the relaxation processes for $Q^{-1}_{>200\,K}$ or $\varepsilon_{a\text{-}I,>200\,K}$ and $\varepsilon_{a\text{-}II,>200\,K}$, and also for the plastic creep. It is not for the GB regions but for the amorphous structures, the following is reported:[28] The nature of inhomogeneities is existing in a computer-built model amorphous metal, and the geometrical coordination numbers extend over several atomic distances and the spatial fluctuations of the shear modulus and atomic volume are quite variable. In the model amorphous metal, with increasing stress, the number of atoms associated with the local structural rearrangements increases at first, and then the percolation like paths for atomic rearrangements develop and the irreversible atomic movements come in. Further, it is not for the GB anelastic relaxation but for the dislocation anelastic relaxation in bcc metals, the strong decrease in the relaxation parameter $1/\tau_0$ with increasing stress is found and assumed to reflect a change in the entropy factor due to the collective motion of many atoms associated with the dislocation motions.[29]

Since the ratio $\varepsilon_{a\text{-}I,>200\,K}/\varepsilon_e$ is the order of 10^{-3} and the fractional volume of the GB regions is about 10% on the assumption that the thickness of the GB region is 1 nm and the mean grain size is 30 nm, the anelastic relaxation process for $Q^{-1}_{>200\,K}$ or $\varepsilon_{a\text{-}I,>200\,K}$ may be explained by localized atomic relaxations associated with not so many atoms. The value of $\varepsilon_{a\text{-}II,>200\,K}$ is comparable with that of ε_e near the room temperature as seen in Fig. 6, and becomes larger than that of ε_e at elevated temperatures.[25] It is suggested that the localized atomic relaxations assumed for $Q^{-1}_{>200\,K}$ or $\varepsilon_{a\text{-}I,>200\,K}$ may not explain such large $\varepsilon_{a\text{-}II,>200\,K}$. Recent molecular dynamics simulation studies for the GB diffusion[30,31] and the GB migration[32,33] reported that the cooperative motion of many atoms can be excited above a certain temperature, which results in a low activation energy and a low pre-exponential factor. We surmise that such the cooperative motion of many atoms accounts for $\varepsilon_{a\text{-}II,>200\,K}$. Further, the threshold stress $\sigma_{a\text{-}II}$ found in the empirical relationship (1) may reflect a barrier for the transition from the localized atomic relaxations for $Q^{-1}_{>200\,K}$ or $\varepsilon_{a\text{-}I,>200\,K}$ to the extended atomic relaxations of $\varepsilon_{a\text{-}II,>200\,K}$.

We also surmise that the further development of the extended atomic motion for $\varepsilon_{a\text{-}II,>200\,K}$ leads to the plastic creep as shown in Fig. 1(c), because the activation energy $E_{pc\text{-}1}$ of 0.36 to 0.55 eV is considerably lower than the activation energy of 0.88 eV reported for the GB diffusion in p-Au.[27] The empirical relationship (2) found for $(d\varepsilon/dt)_{pc\text{-}1}$ is of the grain boundary sliding given by Ashby.[34] However, the value of $(d\varepsilon/dt)_{pc\text{-}1}$ is much lower than that predicted for n-Au with 30 nm after the Ashby model assuming $E_{pc\text{-}1} = 0.88$ eV, indicating that not all the GB regions are associated with the plastic creep for the applied stress below $\sigma_{pc\text{-}2}$.[25] The latter issue is out of the present scope. The present work indicates that the atomic motions in the GB regions in n-Au develop in scale with increasing stress and temperature, and are so different from those in the GB regions in p-Au.

5. Conclusion

For high-density n-Au, various anelastic and plastic creep processes associated with the grain boundary (GB) regions were observed. For the very broad internal friction peak near 95 K, $Q^{-1}_{p,95\,K}$, $1/\tau_0$ of $3 \times 10^{11}\,s^{-1}$ and E of 0.16 eV are found. We surmise that simple relaxation processes are responsible for $Q^{-1}_{p,95\,K}$. Above 200 K, the steep increase in the anelastic strains $\varepsilon_{a\text{-}I,>200\,K}$ and $\varepsilon_{a\text{-}II,>200\,K}$ was activated for the applied stress as low as 0.1 MPa and the applied stress beyond a few MPa, and the linear plastic creep strain $\varepsilon_{pc\text{-}1}$ was activated for the stress range between 30 MPa and 150 MPa, respectively. The values of $1/\tau_0$ and E found for $\varepsilon_{a\text{-}I,>200\,K}$ and $\varepsilon_{a\text{-}II,>200\,K}$ decrease with increasing the applied stress or the temperature. E found for $\varepsilon_{pc\text{-}1}$ is similar to or slightly smaller than that of $\varepsilon_{a\text{-}II,>200\,K}$. These observations indicate that the atomic motions in the GB regions of n-Au develop in scale in the order mentioned above, and are so different from those in the GB regions in p-Au.

Acknowledgements

The authors give thanks Prof. Kita for kind help and valuable discussions. This work is partly supported by the Center for Tsukuba Advanced Research Alliance (TARA) at University of Tsukuba, a Grant in Aid for Scientific Research from the Ministry of Education, Culture, Sports, Science and Technology of Japan, and High Damping Materials Project of

''Research for the Future'' of Japan Society for the Promotion of Science.

REFERENCES

1) H. Gleiter: Prog. Mater. Sci. **33** (1989) 223–315.
2) G. W. Nieman, J. R. Weertman and R. W. Siegel: Scr. Metall. **23** (1989) 2013–2018.
3) J. R. Weertman: Mater. Sci. Eng. A **166** (1993) 161–167.
4) S. Schumacher, R. Birringer, R. Strauß and H. Gleiter: Acta Metall. **37** (1989) 2485–2488.
5) B. S. Bokstein, H. D. Bröse, L. I. Trusov and T. P. Khvostantseva: Nanostruct. Mater. **6** (1995) 873–876.
6) P. G. Sanders, J. A. Eastman and J. R. Weertman: Acta Mater. **45** (1997) 4019–4025.
7) P. G. Sanders, C. J. Youngdahl and J. R. Weertman: Mater. Sci. Eng. A **234–236** (1997) 77–82.
8) S. Sakai, H. Tanimoto and H. Mizubayashi: Acta Mater. **47** (1999) 211–217.
9) H. Tanimoto, S. Sakai and H. Mizubayashi: Mater. Trans., in Press.
10) R. Würschum, K. Reimann and P. Faber: Defect and Diff. Forum **143–147** (1997) 1463–1468.
11) H. Tanimoto, P. Faber, R. Würschum, R. Z. Valiev and H.-E. Schaefer: NanoStruct. Mater. **12** (1999) 681–684.
12) H. Tanimoto, L. Pasqunrni, R. Prümmer, H. Kromüller and H.-E. Schaefer: Scr. Mater. **42** (2000) 961–966.
13) M. Weller, J. Diehl and H.-E. Schaefer: Philos. Mag. A **63** (1991) 527–533.
14) M. J. Lang, M. Duarte-Dominguez, R. Birringer, R. Hempelmann, H. Natter and W. Arnold: Nanostruct. Mater. **12** (1999) 811–816.
15) W. N. Weins, J. D. Makinson, R. J. De Angelis and S. C. Axtell: Nanostruct. Mater. **9** (1997) 509–512.
16) E. Bonetti, L. Pasquini and E. Sampaolesi: Nanostruct. Mater. **10** (1998) 437–448.
17) E. Bonetti, L. Del Bianco, L. Pasquini and E. Sampaolesi: Nanostruct. Mater. **10** (1998) 741–753.
18) E. Bonetti, E. G. Campari, L. Del Bianco, L. Pasquini and E. Sampaolesi: Nanostruct. Mater. **11** (1999) 709–720.
19) B. Cai, Q. P. Kong, P. Cui, H. T. Cong and X. K. Sun: Scr. Mater. **44** (2001) 1043–1048.
20) Y. Z. Wang, P. Cui, X. J. Wu, J. B. Huang and B. Cai: Phys. Status Solidi (a) **186** (2001) 99–104.
21) H. Tanimoto, H. Mizubayashi, H. Fujita and S. Okuda: J. de Phys. **6** (1996) C8-199-202.
22) H. Tanimoto, S. Sakai, K. Otsuka, E. Kita and H. Mizubayashi: Mater. Sci. Engineering, submitted.
23) S. Sakai: Thesis, University of Tsukuba, (2001).
24) S. Sakai, H. Tanimoto, K. Otsuka, T. Yamada, Y. Koda, E. Kita and H. Mizubayashi: Scr. Mater. **45** (2001) 1313–1319.
25) S. Sakai, H. Tanimoto and H. Mizubayashi: Phys. Rev. B, in press.
26) G. Fantozzi, C. Esnouf. W. Benoit and I. G. Ritchie: Prog. Mater. Sci. **27** (1982) 311–451, and references therein.
27) ''Landolt-Börnstein Numerical Data and Functional Relationships in Science and Technology: New Series Group III, Vol. 26'', ed. by H. Mehrer, (1990), p. 630.
28) K. Maeda and S. Takeuchi: J. Phys. F: Met. Phys. **12** (1982) 2767–2781.
29) H. Mizubayashi: Defect and Diffusion Forum **119–120** (1995) 111–126.
30) M. R. Sørensen, Y. Mishin and A. F. Voter: Phys. Rev. B **62** (2000) 3658–3672.
31) P. Keblinski, D. Wolf, S. R. Phillpot and H. Gleiter: Philos. Mag. A **79** (1999) 2735–2761.
32) B. Shönfelder, D. Wolf, S. R. Phillpot and M. Furtkamp: Interface Sci. **5** (1997) 245–262.
33) B. Shönfelder, P. Keblinski, D. Wolf and S. R. Phillpot: Mater. Sci. Forum **294** (1999) 9–16.
34) M. F. Ashby and R. A. Verrall: Acta Metall. **21** (1973) 149–163.